nature portfolio

https://doi.org/10.1038/s41563-021-00937-0

Supplementary information

Efficient and low-voltage vertical organic permeable base light-emitting transistors

– Supplementary Information –

Efficient and low-voltage vertical organic permeable-base light-emitting transistors

Zhongbin Wu[1,2,6]✉, Yuan Liu[2,5,6], Erjuan Guo[2,6], Ghader Darbandy[3], Shu-Jen Wang[2], René Hübner[4], Alexander Kloes[3], Hans Kleemann[2] and Karl Leo[2]

[1]Frontiers Science Center for Flexible Electronics, Institute of Flexible Electronics (IFE), Northwestern Polytechnical University, 127 West Youyi Road, Xi'an 710072, China.
[2]Dresden Integrated Center for Applied Physics and Photonic Materials (IAPP) and Institute for Applied Physics, Technische Universität Dresden, 01062 Dresden, Germany.
[3]NanoP, TH Mittelhessen, University of Applied Sciences, 35390 Giessen, Germany.
[4]Institute of Ion Beam Physics and Materials Research, Helmholtz-Zentrum Dresden-Rossendorf, Bautzner Landstrasse 400, Dresden 01328, Germany.
[5]Present address: Key Laboratory of the Ministry of Education for Optoelectronic Measurement Technology and Instrument, Beijing Information Science & Technology University, Beijing 100192, China.
[6]These authors contributed equally: Zhongbin Wu, Yuan Liu, Erjuan Guo.
✉e-mail: iamzbwu@nwpu.edu.cn

Supplementary Figures:

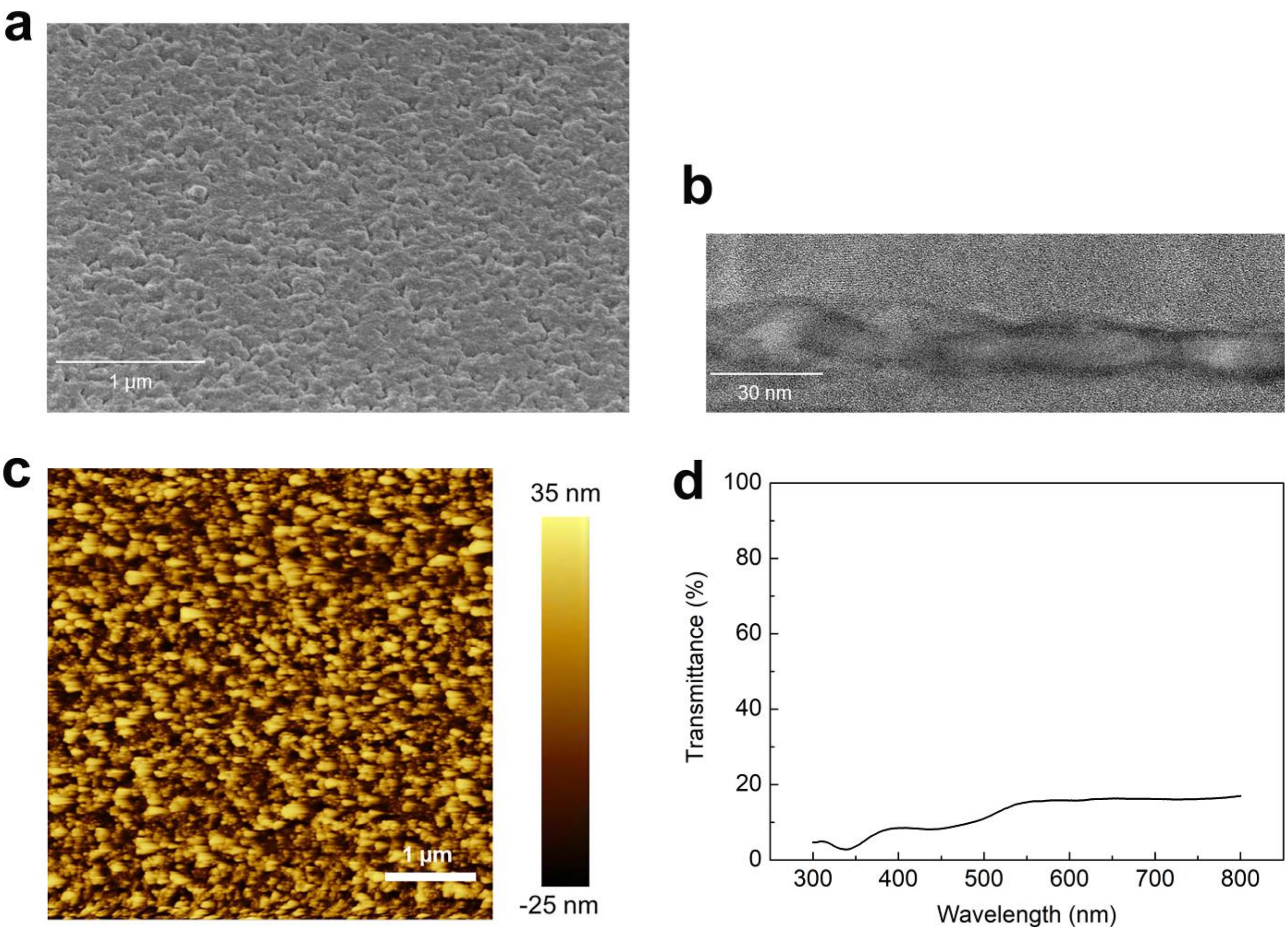

Supplementary Fig. 1 | Characterization of the permeable-base electrode. a, Tilted-view SEM image of the permeable-base electrode Al/AlOx with nanopores across the surface. **b**, Cross-sectional TEM image of the 15-nm-thick base (gate) electrode encapsulated with C_{60} layers for protection. The sample was prepared using a focused ion beam device. **c**, Atomic force microscopy (AFM) image of the surface of the base electrode. The scanned active area is 5 µm × 5 µm. The RMS roughness is about 5 nm. **d**, The transmittance spectrum of the 15-nm-thick Al/AlOx used for the base electrode in OPB-LETs.

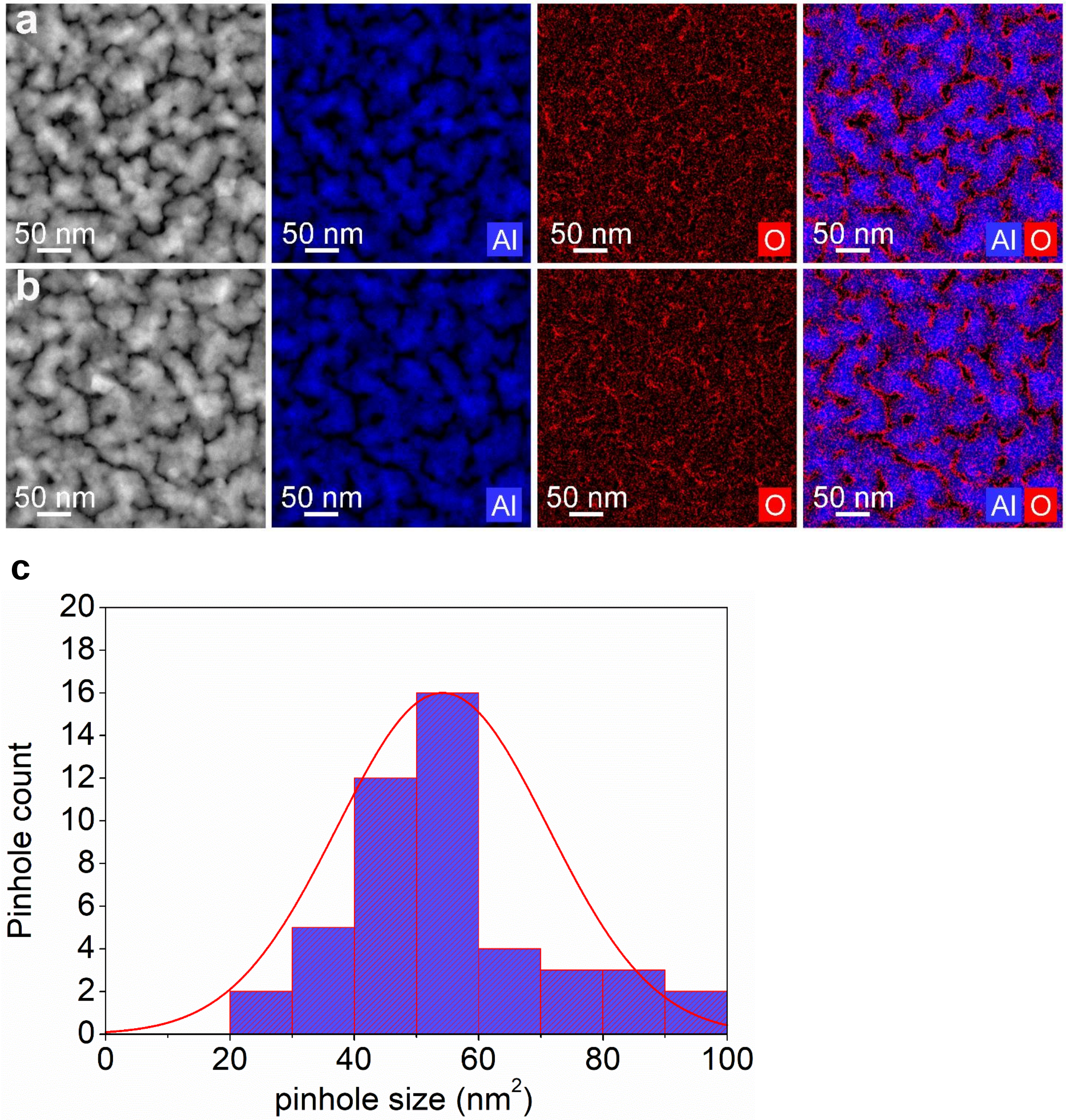

Supplementary Fig. 2 | HAADF-STEM images and the corresponding EDXS analysis of Al/AlOx base electrode. Two different positions (**a**) and (**b**) of the Al/AlOx base electrode are randomly selected. Energy-dispersive X-ray spectroscopy (EDXS) based element maps (Al: blue, O: red) of the base layer show well-passivated pinholes in the metallic film, proving that the sample is uniformly oxidized and the pinholes are free of both elements. **c**, Histogram of the pinhole size distribution.

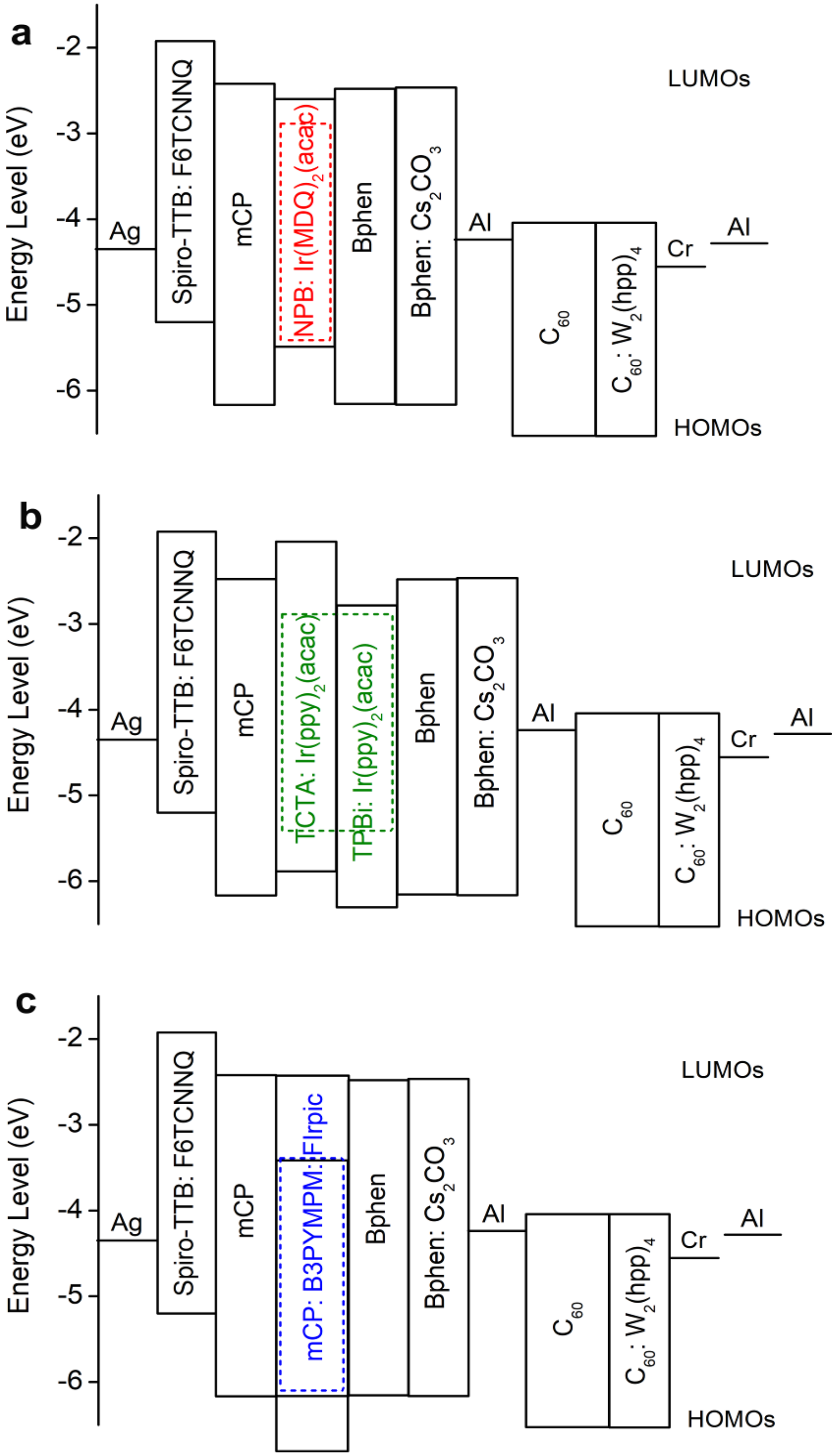

Supplementary Fig. 3 | Appropriate carrier injection barriers for fabricated OPB-LET devices. **a**-**c**, Energy-level diagrams of red (a), green (b), and blue (c) OPB-LET devices. All energy levels are in units of electron volts. The energy levels of all materials are measured by ultraviolet photoelectron spectroscopy (UPS) from our previous reports.

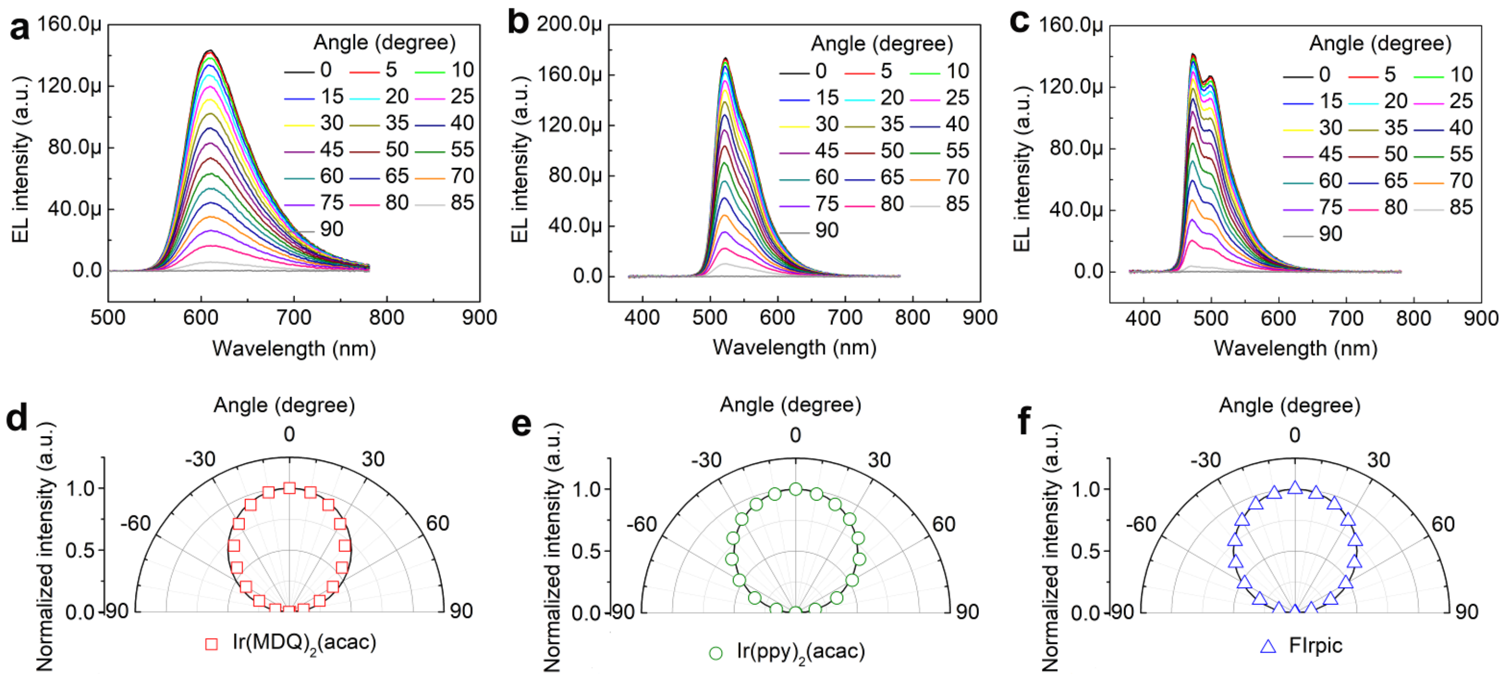

Supplementary Fig. 4 | Angle-dependent electroluminescence spectra of red, green and blue OPB-LETs. **a**-**c**, Electroluminescence spectra measured at different angles. **d**-**f**, Comparison of the angle-dependent EL intensity and the standard Lambertian distribution.

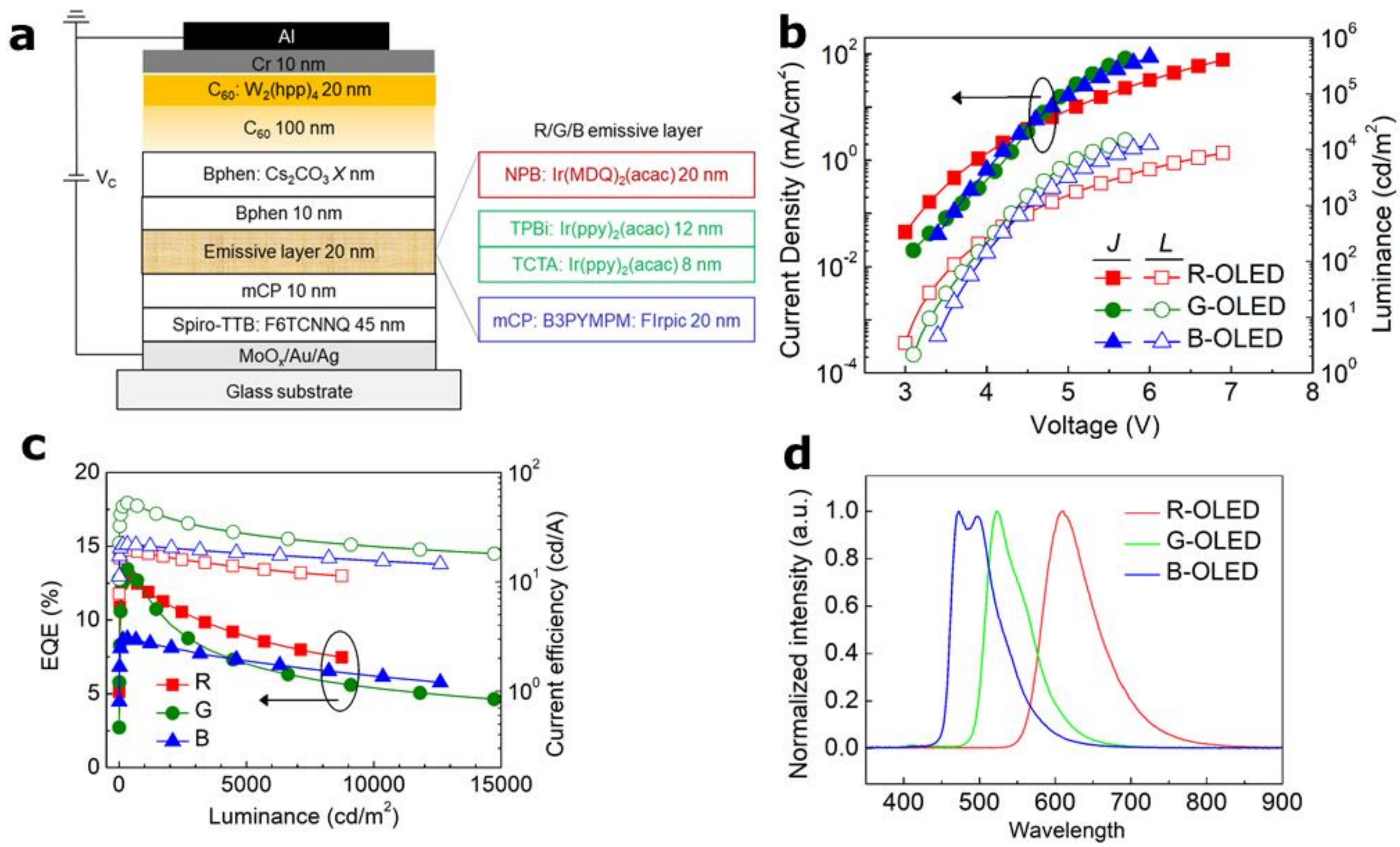

Supplementary Fig. 5 | Device performance of fabricated organic light-emitting devices without Al/AlOx base electrode. a, Device structure of organic light-emitting devices (OLEDs) without the permeable-base electrode. **b**, Current density-voltage-luminance (*J*-*V*-*L*) characteristics of the OLEDs. **c**, External quantum efficiency (EQE) and current efficiency (CE)-luminance characteristics of the OLEDs. **d**, Electroluminescence (EL) spectra of red, green, and blue OLEDs.

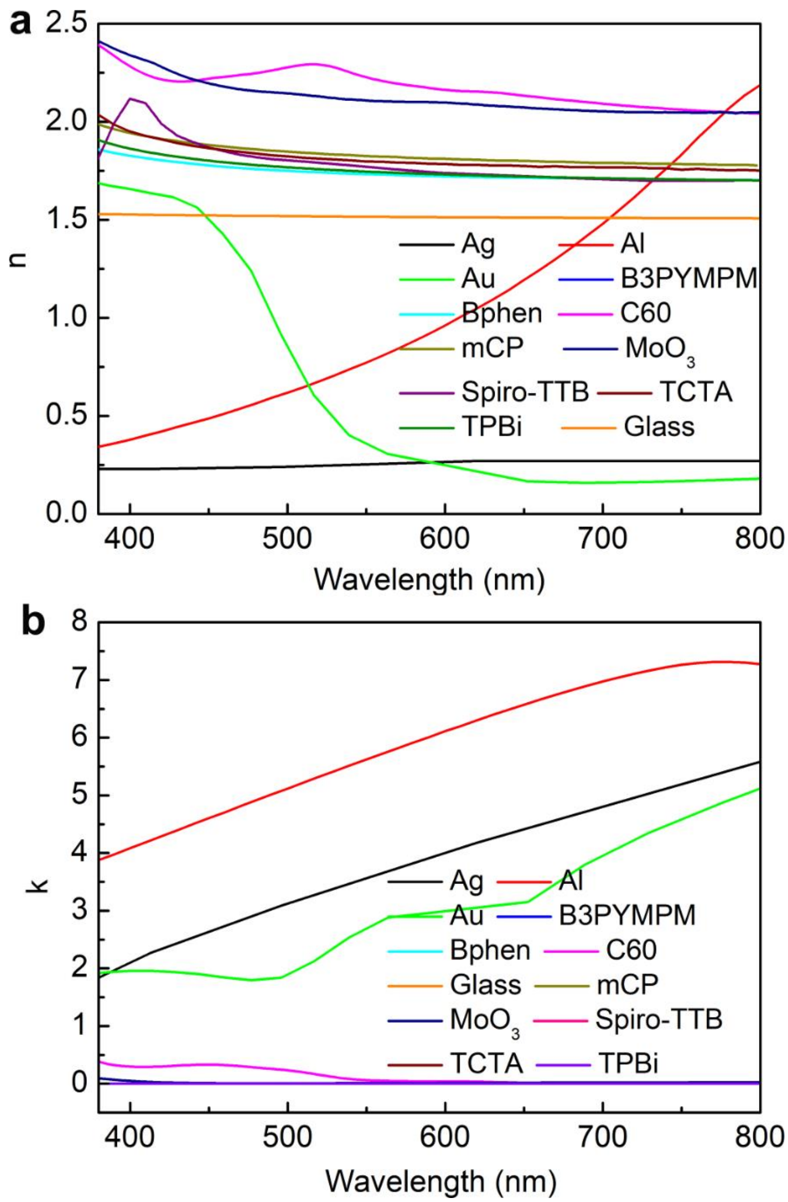

Supplementary Fig. 6 | The refractive index of all the materials used in simulation.

a, *n* values of the used materials. **b**, *k* values of the used materials.

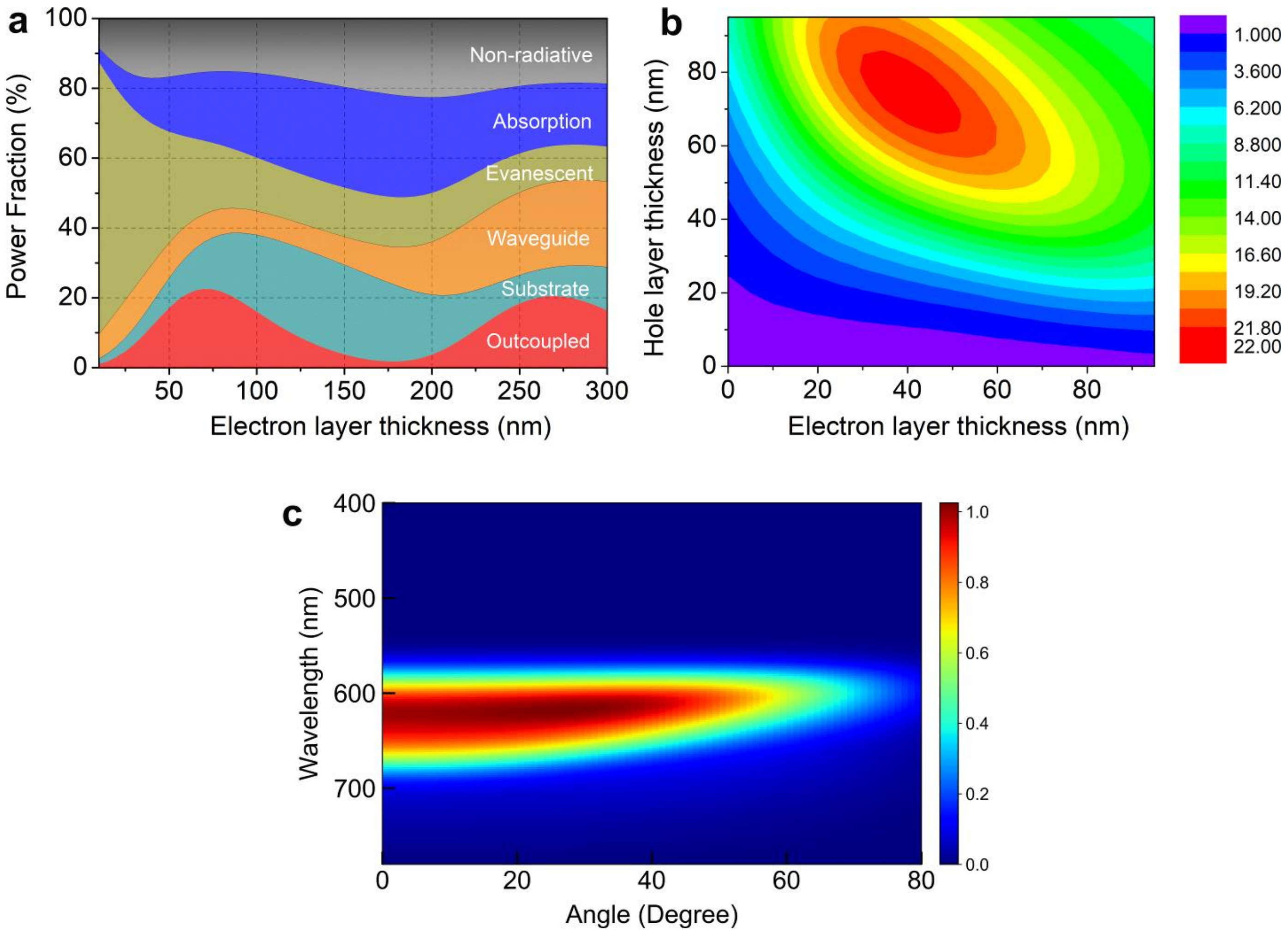

Supplementary Fig. 7 | Optical simulation for photon engineering in red OPB-LETs. **a**, Simulated photon distribution of all loss channels in dependence of the electron layer thickness in red OPB-LETs. Most generated photons go into substrate, waveguided and evanescent modes. **b**, Calculated extraction efficiency from the simulated photon distribution in red OPB-LETs. **c**, Angular-resolved spectral radiant intensity (SRI) of the present devices with the electron-transporting layer thickness of 50 nm at the brightness of 1000 cd m^{-2}. The plot displays the SRI in dependence of the wavelength λ and polar angle θ for red OPB-LETs.

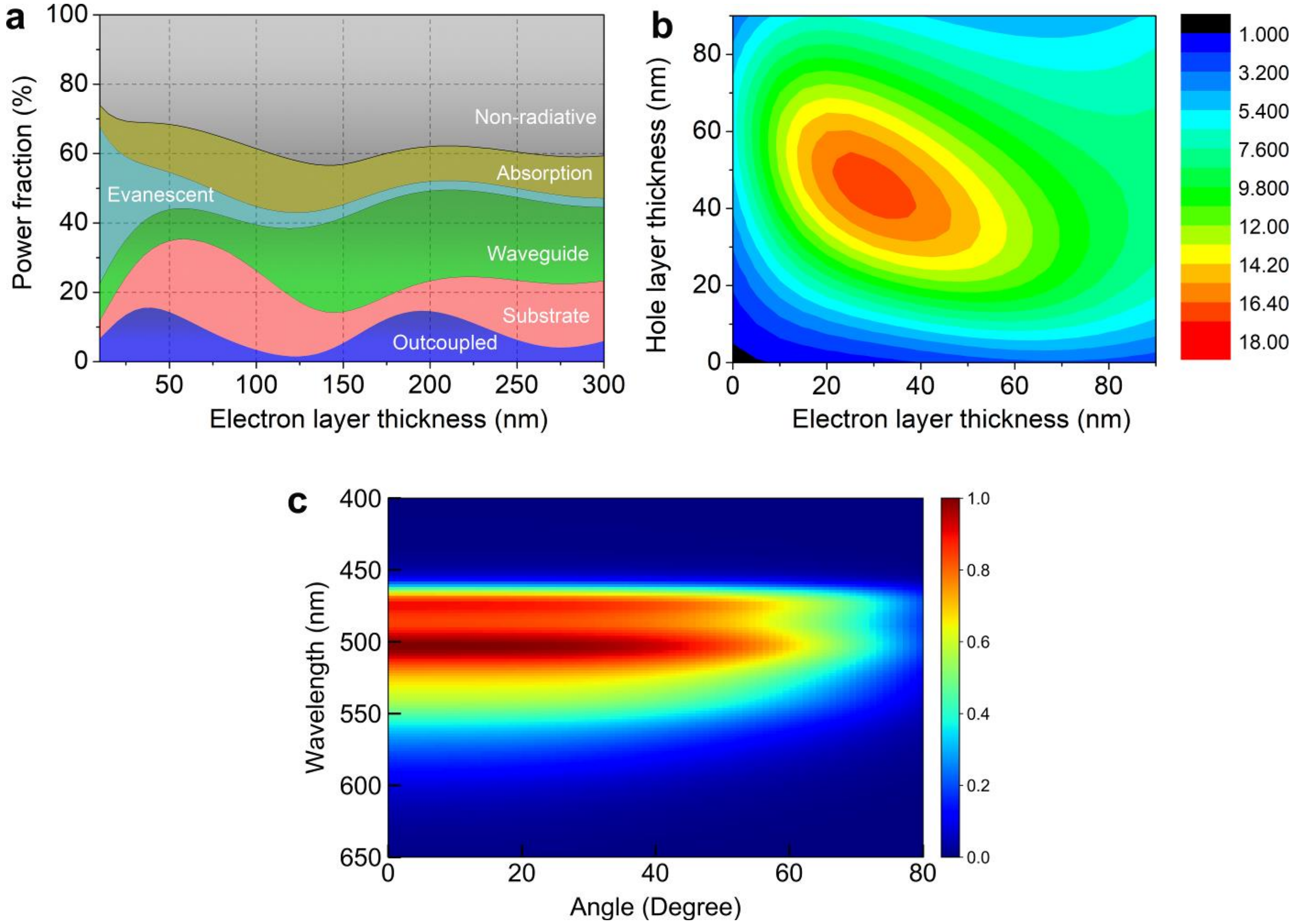

Supplementary Fig. 8 | Optical simulation for photon engineering in blue OPB-LETs. **a**, Simulated photon distribution of all loss channels in dependence of the electron layer thickness in blue OPB-LETs. Most generated photons go into the substrate, waveguided and evanescent modes. **b**, Calculated extraction efficiency from the simulated photon distribution in blue OPB-LETs. **c**, Angular-resolved spectral radiant intensity (SRI) of the present devices with the electron-transporting layer thickness of 50 nm at the brightness of 1000 cd m^{-2}. The plot displays the SRI in dependence of the wavelength λ and polar angle θ for blue OPB-LETs.

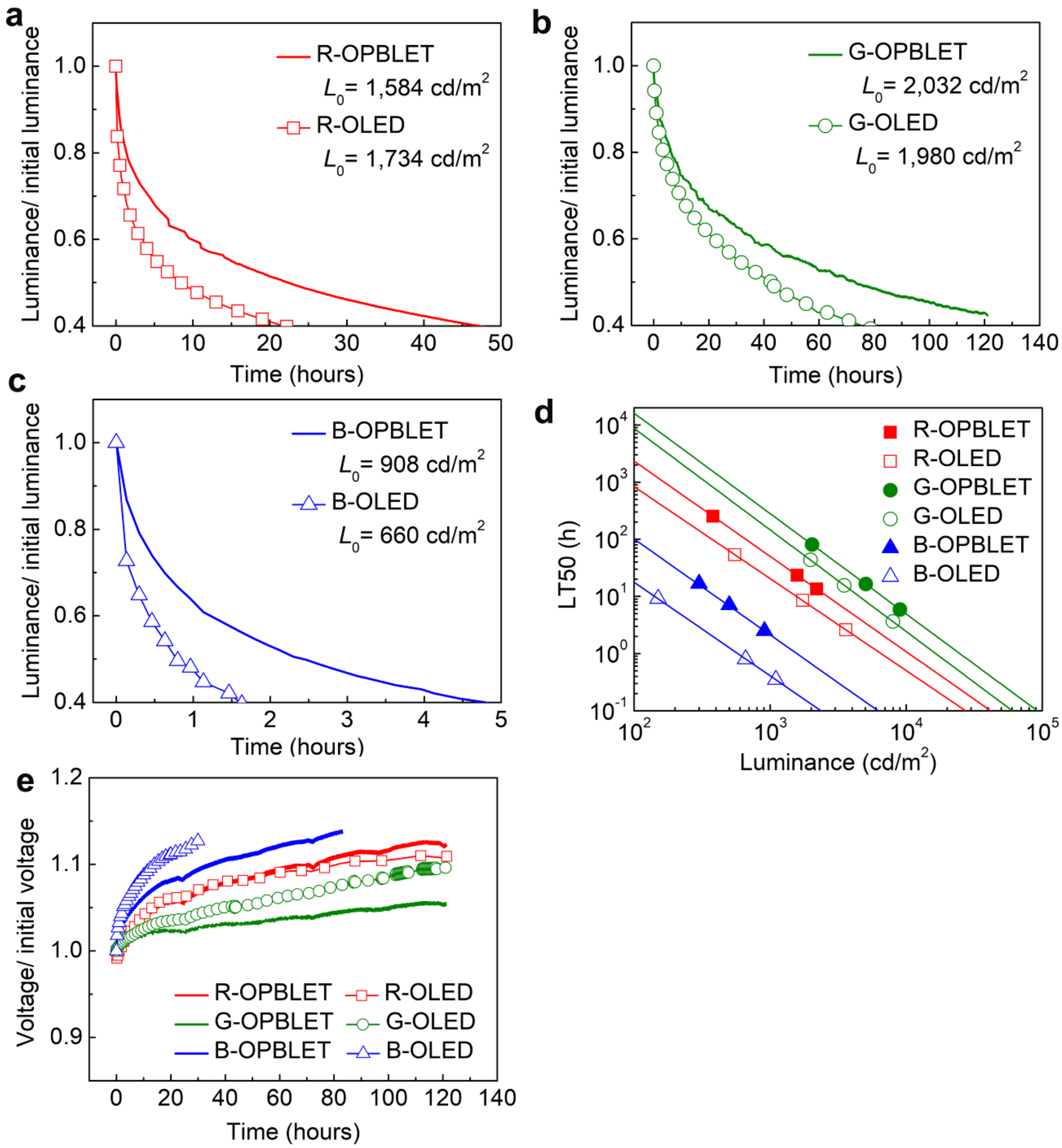

Supplementary Fig. 9 | Operational stability of fabricated OPB-LETs and OLEDs. a-c, Luminance/initial luminance versus time curves of red (**a**), green (**b**), blue (**c**) OPB-LETs and OLEDs, respectively. **d**, LT50 versus initial luminance of all red, green, blue OPB-LETs and OLEDs, respectively, LT50 is defined as the time it takes for the initial luminance to drop to 50%. Lower luminance values *L* will lead to higher lifetimes. **e**, Voltage/initial voltage versus time curves of all red, green, blue OPB-LETs and OLEDs, respectively.

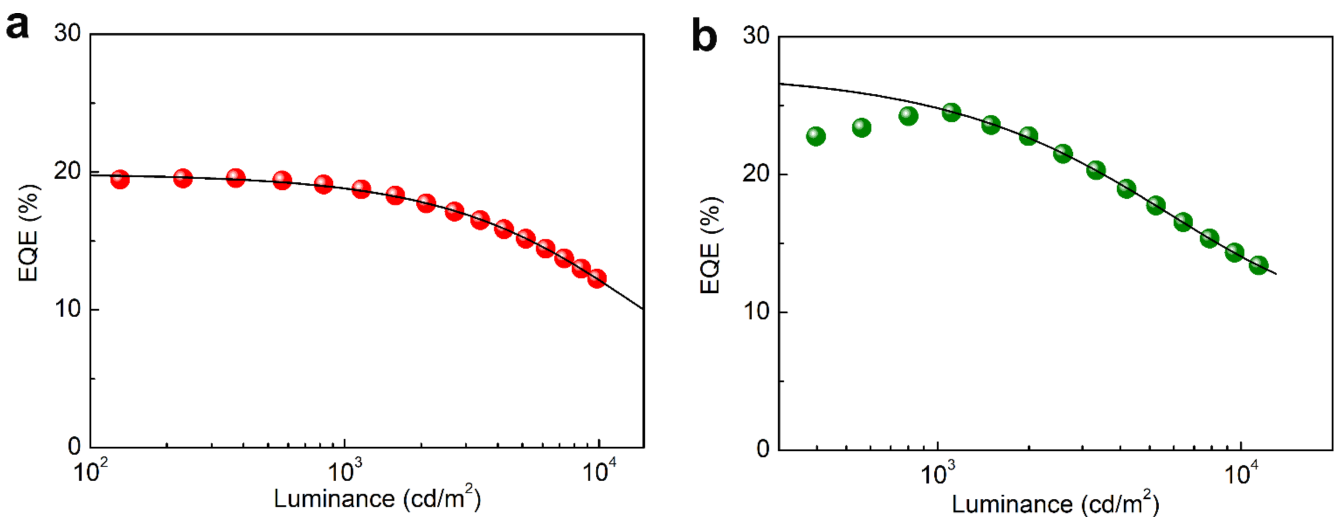

Supplementary Fig. 10 | Efficiency roll-off. **a**, External quantum efficiency (EQE) versus luminance (red circles) and triplet-triplet annihilation (TTA) fitting (black line) in red OPB-LETs. **b**, EQE versus luminance (green circles) and TTA fitting (black line) in green OPB-LETs.

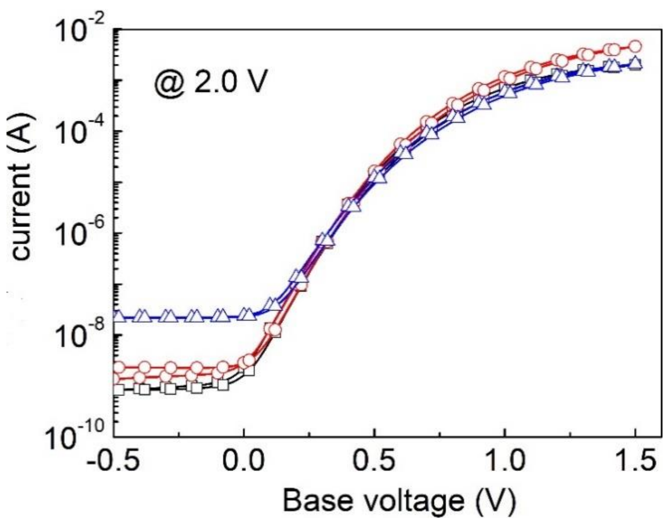

Supplementary Fig. 11 | Hysteresis behavior. Transfer characteristics of three organic permeable-base transistors (forward and backward sweep) as a function of V_B at V_C = 2.0 V, respectively.

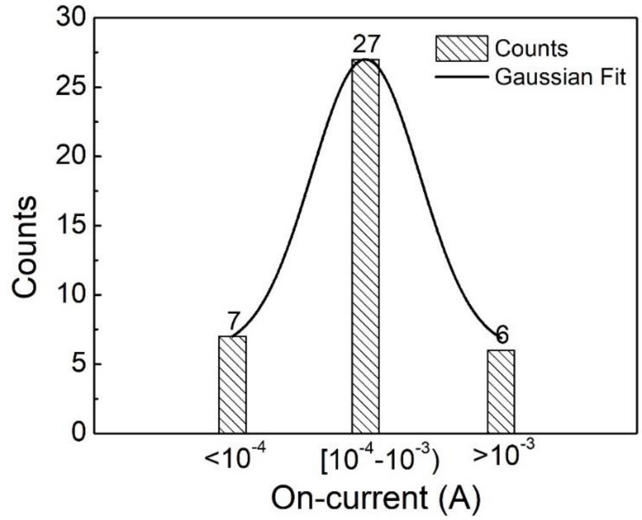

Supplementary Fig. 12 | Device to device reproducibility of OPBTs using air oxidation.

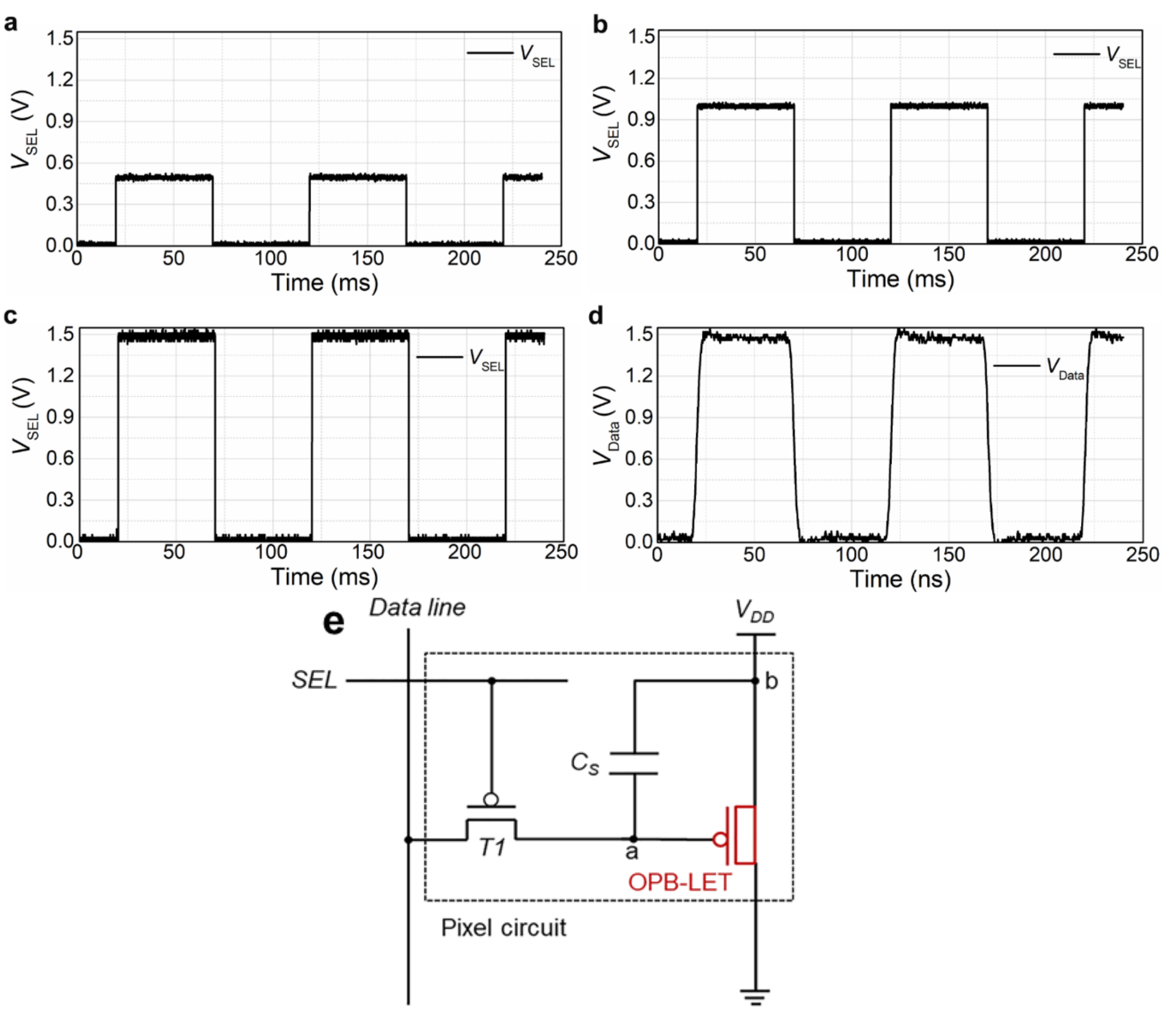

Supplementary Fig. 13 | The display driving demo. To show the integrating capability of the OPB-LETs, the demo consists of an organic permeable-base transistor for the select voltage line and an OPB-LET.

Supplementary Fig. 14 | The pictures of red, green and blue OPB-LET operated at the constant base and collector voltages of 2.0 V and 4.0 V, respectively. It shows that the OPB-LETs using the wet-electrochemical anodization of the base electrode can also work, but the device efficiency is low compared with the devices using air oxidation, because the electrochemical route leads to the strong electrochemical anodization and it also needs high temperature to eliminate the remaining reagent.

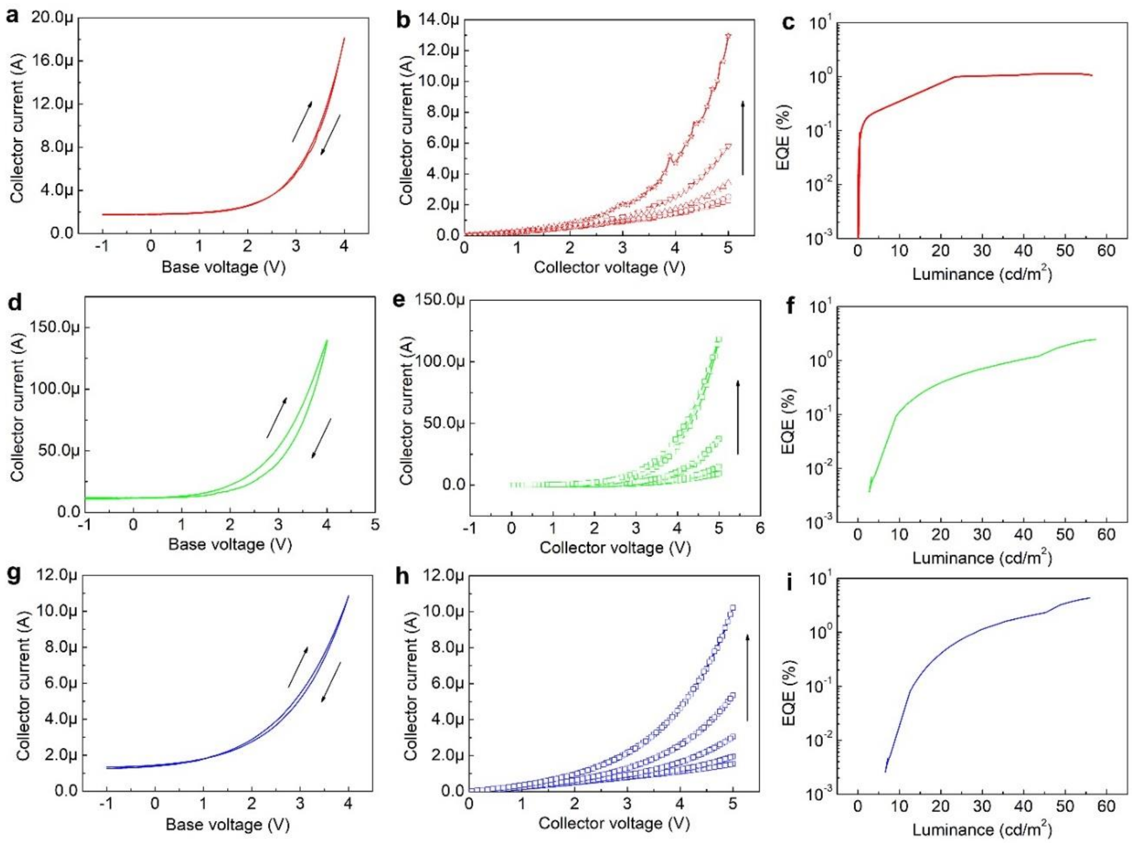

Supplementary Fig. 15 | Device performance of organic permeable-base light-emitting transistors with the base electrode prepared by wet-electrochemical anodization. The transfer and output characteristics of red (**a**, **b**), green (**d**, **e**) and blue (**g**, **h**) OPB-LETs with the forward and backward scan. The external quantum efficiency-luminance curves of red (**c**), green (**f**), and blue (**i**) OPB-LETs.

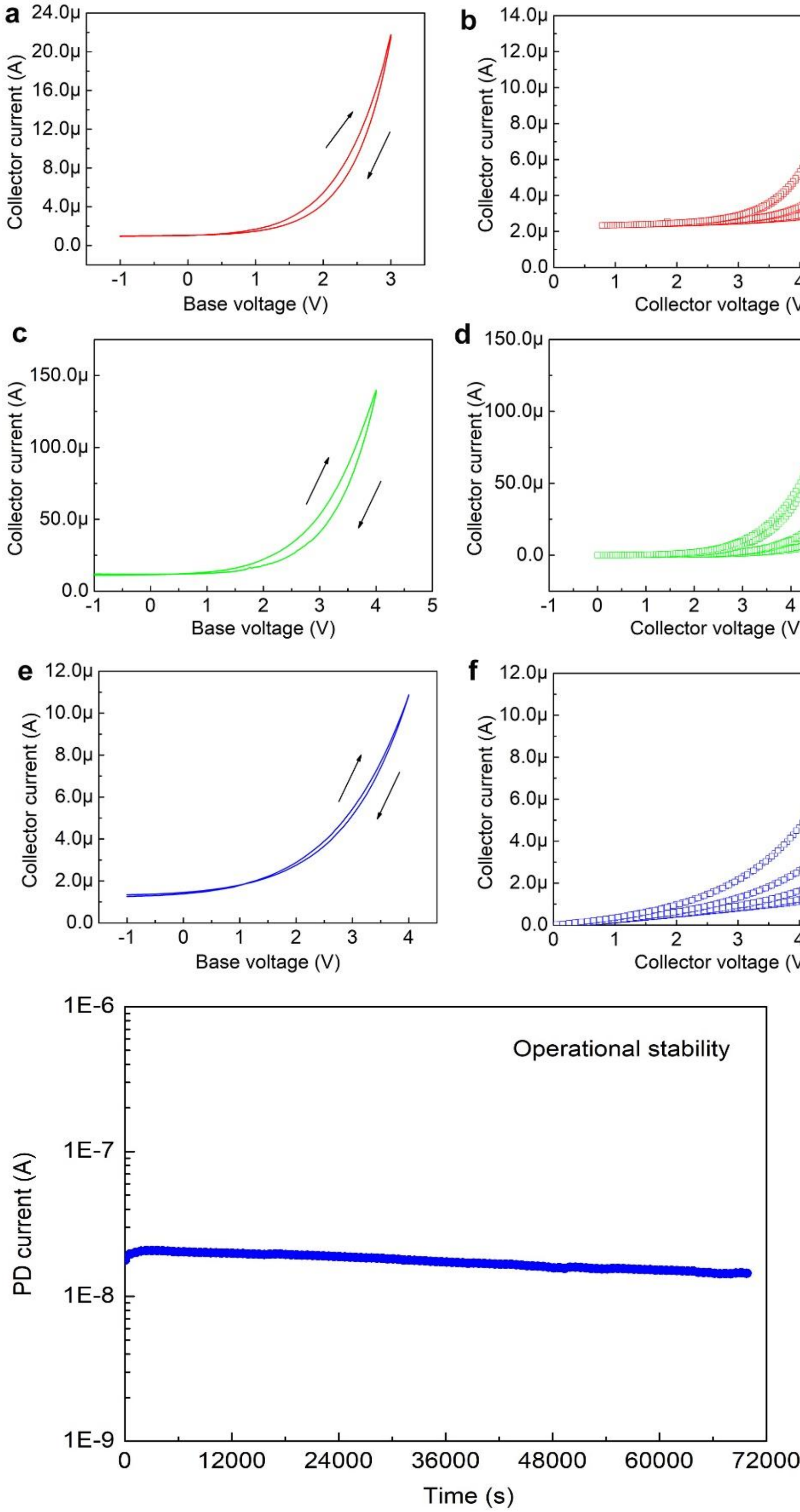

Supplementary Fig. 16 | Device performance of organic permeable-base light-emitting transistors using TPBi as the electron-transporting layer.

Supplementary Notes

Supplementary Note 1: Efficiency roll-off.

The triplet-triplet annihilation (TTA) model follows the established bi-excitonic quenching mechanism. The equation for the TTA fitting is expressed as

$$\frac{\eta_{EQE}}{\eta_0} = \frac{J_0}{4J}\left(\sqrt{1+\frac{8J}{J_0}}-1\right),$$

where η_{EQE} represents the maximum EQE in the absence of TTA, J_0 is the critical current density, which represents the current density at which EQE drops to half of its maximum value, and J is the current density. Our experimental results agree well with the TTA model (see Supplementary Fig. 10).

Supplementary Note 2: Optical simulation.

In the simulation process, we adopt a classical electromagnetic model by treating the radiative dipole as an electrical dipole antenna and utilizing the transfer matrix method. The detailed simulation process can be found in the reference: Furno, M., Meerheim, R., Hofmann, S., Lüssem, B. & Leo, K. Phy. Rev. B 85, 115205 (2012). All the layers used here are isotropic, and the emitting layer does not absorb any light. The refractive index of all the materials used in the simulation is shown in Supplementary Fig. 6. The power fractions of all channels of the red and blue emitters-based OLETs are also shown in Supplementary Figs. 7 and 8.

Supplementary Tables

Supplementary Table 1 | Summary of OLETs with various device architectures. **a**, The maximum luminance, external quantum efficiency, and current efficiency. **b**, The ratio of the luminance at certain voltages between the on- and off-states.

OLET	Ref.	Luminance [cd/m^2][a)]	EQE_{max} [%][a)]	CE_{max} [cd/A][a)]	ON/OFF ratio[b)]
Single layer; vacuum deposition; Tetracene	Ref.S1	45.0	-	0.0024	10^6
Single layer; vacuum deposition;	Ref.S2	3.0	3.0×10^{-4}	-	-
Single layer; vacuum deposition;	Ref.S3	-	3.0×10^{-3}	-	-
Single layer; spin coating;	Ref.S4	-	0.4	-	-
Single layer; spin coating;	Ref.S5	8,000	8.16	28.2	
Single crystal; physical vapor transport	Ref.S6		3.7×10^{-4}	-	-
Single crystal; physical vapor transport	Ref.S7	1,210	1.61	-	-
Single crystal; physical vapor transport	Ref.S7	3,180	1.75	-	-
Bilayer; vacuum deposition	Ref.S8	-	0.12 ~ 0.15	-	-
Trilayer; vacuum deposition	Ref.S9	-	5.0	-	-
Bulk heterojunction; spin coating	Ref.S10	-	1.2	-	-
Hybrid LET; solution process	Ref.S11	700	0.01	-	5×10^2
TADF OLET; solution process	Ref.S12	1,500	1.0	-	10^5
Semitransparant, solution process	Ref.S13	750	1.7	-	10^4
TADF OLET; svacuum deposition	Ref.S14	14,500	9.01	-	10^5
Multilayer OLET; solution+vacuum deposition	Ref.S15	8,000	10.3	-	10^5
Dual-gate OLET	Ref.S16	2,190	5.7	-	10^5
Trilayer; solution process	Ref.S17	-	2.8	-	10^5
Vertical; spin coating	Ref.S18	500	-	-	10^4
Vertical; vacuum deposition; porous ITO	Ref.S19	170	-	-	10^4
Vertical; vacuum deposition	Ref.S20	29.4	-	-	5×10^3
Vertical; vacuum deposition; MIS	Ref.S21	1,034	-	~ 1.0	10^4
Vertical; vacuum+solution process; nanotube; red	Ref.S22	~ 1,000	-	12.5	10^4
Vertical; vacuum+solution process; nanotube; blue	Ref.S22	~ 1,000	-	23.3	10^4
Vertical; vacuum+solution process; nanotube; green	Ref.S22	~ 2,000	-	48.0	10^4
Vertical; vacuum deposition; permeable base; red	This work	9,833	19.6	20.6	10^5
Vertical; vacuum deposition; permeable base; blue	This work	4,753	11.8	27.1	10^4
Vertical; vacuum deposition; permeable base; green	This work	12,513	24.6	90.1	10^5

Supplementary Table 2 | Summary of lifetime (*LT_{50}*) of OPB-LETs and OLEDs at 1,000 cd/m^2 and 100 cd/m^2. LT_{50} is defined as the time when the luminance drops to half of the initial value. The devices encapsulated are measured in ambient air. $(L_0)^n LT_{50}$= constant, the acceleration factor n values are calculated (Fig. S9 in Supplementary Information).

Devices	n value	LT_{50} at 1,000 cd/m^2	LT_{50} at 100 cd/m^2
Red-OPBLET	1.67	50.2 h	2,349.3 h
Red-OLED	1.65	21.1 h	941.6 h
Green-OPBLET	1.73	275.2 h	14,776.8 h
Green-OLED	1.75	143.8 h	8,084.5 h
Blue-OPBLET	1.74	2.1 h	116.1 h
Blue-OLED	1.73	0.4 h	30.0 h

Supplementary Table 3 | Summary of aperture ratios and power consumption of present display technologies.

Devices	Reference	Effective aperture ratio†	Parasitic power dissipation‡
TFT+OLED	Jpn. J. Appl. Phys. Part 1 44, 3678 (2005)	50%	53%
IGZO+OLED	J. Soc. Inf. Display 28, 350 (2020)	-	> 40%
LTPS+OLED	J. Soc. Inf. Display 28, 350 (2020)	-	> 40%
MIS-OLET	Jpn. J. Appl. Phys. 47, 1889 (2008)	45%	51%
SWCNT-OLET	Science 332, 570-573 (2011)	98%	6.2%
OPB-LET	This work	98%	3.5%

†This parameter excludes the switching TFT and addressing lines; ‡Percentage of power dissipated across the driving transistor portion of the device not contributing to light generation, the values of the commercial IGZO/LTPS+OLED are from the full display.

Supplementary Table 4 | Full names of the chemical molecules used.

Acronym	Full name	Function
Spiro-TTB	Spiro-tetra(p-methyl-phenyl)-benzidine	Hole-transporting
mCP	N,N´-dicarbazolyl-1,3-benzene	Exciton blocking
NPB	N,N'-Di(naphthalene-2-yl)-N,N'diphenyl-benzidine	Host
F6TCNNQ	2,2'-(perfluoronaphthalene-2,6-diylidene)dimalononitrile	p-dopant
Bphen	4,7-diphenyl-1,10-phenanthroline	Electron-transporting
TCTA	4,4',4''-tris(carbazol-9-yl)-triphenylamine	Host
$Ir(ppy)_2(acac)$	Bis(2-phenylpyridine)iridium(III) acetylacetonate	Green emitter
$Ir(MDQ)_2(acac)$	Iridium(III)bis(2-methyldibenzo-[f,h]chinoxalin)(acetylacetonat)	Red emitter
FIrpic	iridium(III)bis[(4,6-difluorophenyl)-pyridinato-N,C2]picolinate	Blue emitter
C_{60}	Buckminster Fullerene	Electron-transporting
TPBi	1,3,5-Tris(1-phenyl-1Hbenzimidazol-2-yl)benzene	Co-host
$W_2(hpp)_4$	tetrakis(1,3,4,6,7,8-hexahydro-2H-pyrimido[1,2-a]pyrimidinato)ditungsten (II)	n-dopant
B3PYMPM	4,6-Bis(3,5-di(pyridin-3-yl)phenyl)-2-MethylpyriMidine	Co-host

Supplementary Videos

Supplementary Video 1：

This video shows the on/off switching function of the OPB-LETs, here we use a blue OPB-LET as the example.

Supplementary Video 2：

This video shows the luminance variation of a blue OPB-LET device. According to Supplementary Fig. 13, to show the integrating capability of the OPB-LETs, the display driving demo consists of a blue OPB-LET and a vertical OPBT for the select voltage line. V_{SEL} increases from 0.5 V to 1.0 V and finally to 1.5 V, $V_{\_Data}$ = 1.5 V.

References:

S1 Hepp, A. et al. Light-emitting field-effect transistor based on tetracene thin film. *Phys. Rev. Lett.* **91**, 157406 (2003).

S2 Sakanoue, T., Yahiro, M., Adachi, C., Burroughes, J. H., Oku, Y., Shimoji, N., Takahashi, T. & Toshimitsu, A. Alignment-free process for asymmetric contact electrodes and their application in light-emitting organic field-effect transistors *Appl. Phys. Lett.* **92**, 053505 (2008).

S3 Zaumseil, J., Friend, R. H. & Sirringhaus, H. Spatial control of the recombination zone in an ambipolar light-emitting organic transistor. *Nat. Mater.* **5**, 69–74 (2005).

S4 Zaumseil, J., McNeill, C. R., Bird, M., Smith, D. L., Ruden, P. P., Roberts, M., McKiernan, M. J., Friend, R. H. & Sirringhaus, H. Quantum efficiency of ambipolar light-emitting polymer field-effect transistors. *J. Appl. Phys.* **103**, 064517 (2008).

S5 Gwinner, M. C., Kabra, D., Roberts, M., Brenner, T. J. K., Wallikewitz, B. H., McNeill, C. R., Friend, R. H. & Sirringhaus, H. Highly efficient single-layer polymer ambipolar light-emitting field-effect transistors. *Adv. Mater.* **24**, 2728 (2012).

S6 Yamao, T., Sakurai, Y., Terasaki, K., Shimizu, Y., Jinnai, H. & Hotta, S. Current-injected spectrally-narrowed emissions from an organic transistor. *Adv. Mater.* **22**, 3708 (2010).

S7 Qin Z. et al. High-efficiency single-component organic light-emitting transistors. *Adv. Mater.* **31**, 1903175 (2019).

S8 Feldmeier, E. J., Schidleja, M., Melzer, C. & Seggern, H. V. A color-tuneable organic light-emitting transistor *Adv. Mater.* **22**, 3568 (2010).

S9 Capelli, R. et al. Organic light-emitting transistors with an efficiency that outperforms the equivalent light-emitting diodes. *Nat. Mater.* **9**, 496–503 (2010).

S10 Chang, J. F., Gwinner, M. C., Caironi, M., Sakanoue, T. & Sirringhaus, H. Conjugated-polymer-based lateral heterostructures defined by high-resolution photolithography. *Adv. Funct. Mater.* **20**, 2825 (2010).

S11 Chaudhry, M. et al. Low-voltage solution-processed hybrid light-emitting transistors. *ACS Appl. Mater. Interfaces* **10**, 18445−18449 (2018).

S12 Ahmad, V. et al. High EQE and high brightness solution-processed TADF light-emitting transistors and OLEDs, *Adv. Optical Mater.*, 2000554 (2020).

S13 Mujeeb, U. et al. Semitransparent and low-voltage operating organic light-emitting field-effect transistors processed at low temperatures. *Adv. Optical Mater.* **4**, 1022–1026 (2016).

S14 Chen, H. et al. Highly efficient flexible organic light emitting transistor based on high-k polymer gate dielectric. *Adv. Opt. Mater.* **8**, 1901651 (2020).

S15 Hu, Y. Improving the efficiency of multilayer organic light-emitting transistors by exploring the hole blocking effect. *Adv. Mater. Interfaces* **2020**, 2000657.

S16 Lee, J.-H. et al. Overlapping-gate organic light-emitting transistors. *Adv. Electron. Mater.* **5**, 1800437 (2019).

S17 Yuan, D. et al. Highly emissive semi-ladder-type copolymers, aggregation state, and solution-processed organic light-emitting transistor. *Chem. Mater.* **32**, 4672−4680 (2020).

S18 Yu, H., Ho, S., Barange, N., Larrabee, R. & So, F. Semi-transparent vertical organic light-emitting transistors. *Org. Electron.* 55, 126 (2018).

S19 Yu, H., Dong, Z., Guo, J., Kim, D. & So, F. Vertical organic field-effect transistors for integrated optoelectronic applications, *ACS Appl. Mater. Interfaces* **8**, 10430-10435 (2016).

S20 Lee, G., Lee, I.-H., Park, H.-L., Lee, S.-H., Han, J., Lee, C., Keum, C.-M. & Lee, S.-D. Vertical organic light-emitting transistor showing a high current on/off ratio through dielectric encapsulation for the effective charge pathway. *J. Appl. Phys.* **121**, 024502 (2017).

S21 Nakamura, K. et al., Improvement of metal–insulator–semiconductor-type organic light-emitting transistors. *Jpn. J. Appl. Phys.* **47**, 1889 (2008).

S22 McCarthy, M. A. et al. Low-voltage, low-power, organic light-emitting transistors for active matrix displays. *Science* **332**, 570-573 (2011).